Edge states of mechanical diamond and its topological origin

2017 New J. Phys. 19 035003

(http://iopscience.iop.org/1367-2630/19/3/035003)

New Journal of Physics
The open access journal at the forefront of physics

Deutsche Physikalische Gesellschaft DPG
IOP Institute of Physics

Published in partnership with: Deutsche Physikalische Gesellschaft and the Institute of Physics

OPEN ACCESS

RECEIVED
8 December 2016

REVISED
3 February 2017

ACCEPTED FOR PUBLICATION
7 February 2017

PUBLISHED
28 March 2017

PAPER

Edge states of mechanical diamond and its topological origin

Yuta Takahashi[1], **Toshikaze Kariyado**[2] **and Yasuhiro Hatsugai**[1]

[1] Graduate School of Pure and Applied Science, University of Tsukuba, Tsukuba 305–8571, Japan
[2] International Center for Materials Nanoarchitectonics (WPI-MANA), National Institute for Materials Science, Tsukuba 305–0044, Japan

E-mail: takahashi@rhodia.ph.tsukuba.ac.jp

Keywords: winding number, edge states, bulk-edge correspondence, Berry phase

Abstract

A mechanical diamond, with the classical mechanics of a spring-mass model arrayed on a diamond lattice, is discussed topologically. Its frequency dispersion possesses an intrinsic nodal structure in the three-dimensional Brillouin zone (BZ) protected by the chiral symmetry. Topological changes of the line nodes are demonstrated, associated with the modification of the tension. The line nodes projected into two-dimensional BZ, form loops, which are characterized by the quantized Berry phases with 0 or π. With boundaries, the edge states are discussed in relation to the Berry phases and winding numbers, and the bulk-edge correspondence of the mechanical diamond is established.

1. Introduction

Topological semimetal is a system in which the band gap is finite almost everywhere in the Brillouin zone, except in some sets of isolated points. In short, it is a system with singular gapless points [1]. Generally, the existence of a singular gapless point leads to nontrivial topology. That is, a singularity often serves as the source of a 'twist' of Bloch wave functions captured by the Berry curvature, giving rise to nontrivial topology. When a system is characterized by a point-like singularity associated with linear dispersion—i.e. a Dirac cone—it is a Dirac/Weyl semimetal, which is a representative topological semimetal [2–6]. Very recently, other kinds of topological semimetals—like nodal line semimetals where the gapless points form a line, which is typically a closed loop—have begun to attract attention as a new stage for playing with topology [7]. Just as in the case of fully gapped topological insulators, topological semimetals are characterized by topologically protected edge modes as a consequence of the bulk-edge correspondence [8].

There have also been intensive efforts to export the idea of topological insulators and topological semimetals to the classical world [9–14]. In particular, classical mechanical systems are interesting playgrounds because of their simplicity and flexibility for tuning parameters [11–13, 15–22]. In fact, we have already seen topological edge modes in various mechanical systems, including photonic and opto-mechanical systems [11–13, 16–19, 23–26]. One specific example which shows this easy-to-tune feature is *mechanical graphene*, which is a honeycomb spring-mass model [17, 19, 27–29]. In mechanical graphene, Dirac cones are known to exist, and their number and position in the Brillouin zone can be controlled by simply changing the tension of the springs in equilibrium [28]. It is worth noting that the effect of the equilibrium tension can be interpreted as spin–orbit coupling if it is clockwise, and the counterclockwise motion of the mass point is mapped to the spin [30, 31].

In this paper, we perform an analysis on a spring-mass model with a diamond structure, namely, a *mechanical diamond*, which is a natural extension of mechanical graphene to three-dimensions [28]. A mechanical diamond is a typical classical nodal line semimetal counterpart. It is revealed that the equilibrium tension induces the unique evolution of the structure of the gapless line nodes. The topological properties of the mechanical diamond are also investigated by relating the edge modes, the quantized Berry phase, and the winding number. In accordance with the unique line node structure, the edge modes also show unique distribution on the surface of the Brillouin zone, including situations with an edge mode multiplicity of 2 or 3. We confirm that these features are well captured by the quantized Berry phase and the winding number, establishing the bulk-edge correspondence in the mechanical diamond. Note that we are dealing with in-gap flat

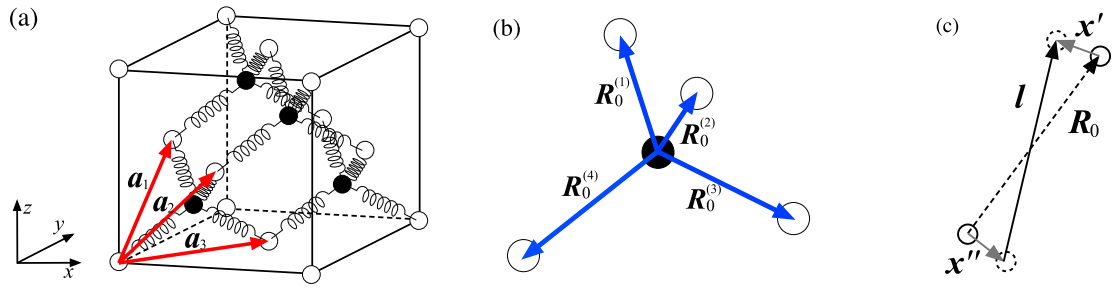

Figure 1. (a) A schematic picture of a mechanical diamond. The unit translation vectors are also shown as $\boldsymbol{a}_i$; (b) the nearest-neighbor vectors $\boldsymbol{R}_0^{(i)}$; (c) the definitions of $\boldsymbol{R}_0$, $\boldsymbol{x}'$ and $\boldsymbol{x}''$.

band edge modes in a chiral symmetric model, not with quantum-Hall-like dispersive edge modes connecting lower and upper bands [32].

The paper is organized as follows: in section 2, the basic notions of the mechanical diamond are explained; then, the frequency dispersion is shown in section 3. Section 4 is devoted to the topological arguments, and the paper is summarized in section 5.

2. Formulation

Let us introduce our model: a *mechanical diamond* consists of mass points aligned in a diamond structure, and springs connecting the nearest-neighbor pairs of the mass points (see figure 1(a)). This three-dimensional model is a natural extension of two-dimensional *mechanical graphene* [28], which is a spring-mass model with a honeycomb structure. As in the case of 2D mechanical graphene, the parameters characterizing our model are the mass of mass points m (m is fixed to a unit for simplicity), the spring constant κ, the natural length of the springs l_0 and the distance between the neighboring mass points R_0. Note that R_0 and l_0 do not necessarily match each other; i.e. R_0 can be larger than l_0 if we apply a proper boundary condition to exert uniform outward tension to the system. In order to investigate the dynamics of the system, we introduce a quantity $\boldsymbol{x}_{\boldsymbol{R}a} = {}^t(x_{\boldsymbol{R}a}, y_{\boldsymbol{R}a}, z_{\boldsymbol{R}a})$ describing the displacement of each mass point from the equilibrium position. Here, $\boldsymbol{R}$ designates the lattice points and a is the sublattice index.

We assume that the elastic energy U_s of a specific spring can be expressed as $U_s = \frac{1}{2}\kappa(l - l_0)^2$ with $l = |\boldsymbol{R}_0 + \boldsymbol{x}' - \boldsymbol{x}''|$, where $\boldsymbol{x}'$, $\boldsymbol{x}''$, and $\boldsymbol{R}_0$ are two displacement vectors for two mass points, and a vector connecting the two equilibrium positions, respectively. By expanding U_s up to the second order in $\delta\boldsymbol{x} = \boldsymbol{x}' - \boldsymbol{x}''$, we obtain

$$U_s \simeq \frac{1}{2}\kappa((R_0 - l_0)^2 + 2(R_0 - l_0)\hat{\boldsymbol{R}}_0 \cdot \delta\boldsymbol{x} + \delta x_\mu \gamma_{\boldsymbol{R}_0}^{\mu\nu} \delta x_\nu), \tag{1}$$

where $\gamma_{\boldsymbol{R}_0}^{\mu\nu} = (1 - \eta)\delta^{\mu\nu} + \eta \hat{R}_0^{\ \mu} \hat{R}_0^{\ \nu}$, $\hat{\boldsymbol{R}}_0 = \boldsymbol{R}_0/|\boldsymbol{R}_0|$ and $\eta \equiv l_0/R_0$. Here, we implicitly take the summation over μ and ν, which run through the directions of the displacement x, y, and z; i.e. we apply the Einstein summation convention. The second term that is linear in $\delta\boldsymbol{x}$ makes no contribution to Newton's equation of motion, as far as we focus on displacement from the equilibrium point, since the linear terms cancel each other out in the equation of motion. The third term is characterized by the parameter η. For $\eta = 1$, at which the springs have a natural length in equilibrium, the angle between $\boldsymbol{R}_0$ and $\delta\boldsymbol{x}$ has a significant impact on the elastic energy because of the factor $\hat{R}_0^{\ \mu} \hat{R}_0^{\ \nu}$. On the other hand, for $\eta = 0$, the limiting case of the stretched springs in equilibrium, U_s, has no dependence on the direction of $\delta\boldsymbol{x}$, in contrast with the case of $\eta = 1$. Therefore, the parameter η enables us to tune the property of the spring-mass model.

For a mechanical diamond, the equation of motion can be derived by evaluating the elastic energy substituting $\boldsymbol{R}_0^{(i)}$ in figure 1(b) into equation (1). If we further assume that the system is periodic in space and time, i.e. by introducing $\phi_{a\mu}(\boldsymbol{k})$ as $u_{\boldsymbol{k}a}^{\mu} = \mathrm{e}^{\mathrm{i}\omega t}\phi_{a\mu}(\boldsymbol{k})$ and $x_{\boldsymbol{R}a}^{\mu} = \frac{1}{N}\sum_{\boldsymbol{k}} \mathrm{e}^{\mathrm{i}\boldsymbol{k}\cdot\boldsymbol{R}} u_{\boldsymbol{k}a}^{\mu}$, the equation of motion reduces to

$$-\omega^2 \phi_{a\mu}(\boldsymbol{k}) + \sum_b \Gamma_{ab}^{\mu\nu}(\boldsymbol{k})\phi_{b\nu}(\boldsymbol{k}) = 0, \tag{2}$$

where $\Gamma_{ab}^{\mu\nu}(\boldsymbol{k}) = (\hat{\Gamma}_{\boldsymbol{k}})_{a\mu;b\nu}$,

$$\hat{\Gamma}(\boldsymbol{k}) = \kappa\left(4 - \frac{8}{3}\eta\right)\hat{1} + \begin{pmatrix} \hat{0} & \hat{\Gamma}_{AB}(\boldsymbol{k}) \\ \hat{\Gamma}_{AB}^{\dagger}(\boldsymbol{k}) & \hat{0} \end{pmatrix}, \tag{3}$$

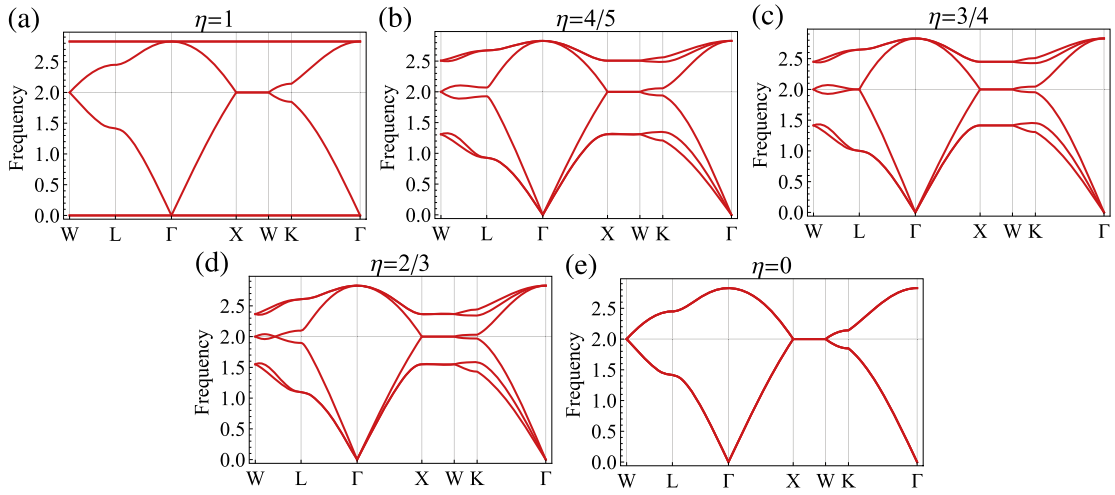

Figure 2. Band structure for (a) $\eta = 1$, (b) $\eta = \frac{4}{5}$, (c) $\eta = \frac{3}{4}$, (d) $\eta = \frac{2}{3}$ and (e) $\eta = 0$.

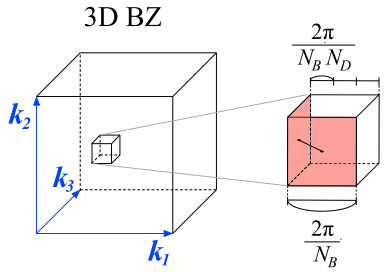

Figure 3. A schematic picture of drawing a line; the red surfaces indicate the Berry phase over the edge of the surface equaling π.

and $\hat{\Gamma}_{AB}(\boldsymbol{k}) = -\kappa(\hat{\gamma}_4 + e^{-i\boldsymbol{k}\cdot\boldsymbol{a}_1}\hat{\gamma}_1 + e^{-i\boldsymbol{k}\cdot\boldsymbol{a}_2}\hat{\gamma}_2 + e^{-i\boldsymbol{k}\cdot\boldsymbol{a}_3}\hat{\gamma}_3)$, with $\hat{\gamma}_i \equiv \hat{\gamma}_{\boldsymbol{R}_0^{(i)}}$ $(i = 1, 2, 3, 4)$ (see figures 1(a) and (b)). The eigenfrequency and the eigenmodes are calculated by diagonalizing $\hat{\Gamma}(\boldsymbol{k})$. Note that $\hat{\Gamma}'(\boldsymbol{k}) = \hat{\Gamma}(\boldsymbol{k}) - \kappa(4 - \frac{8}{3}\eta)\hat{1}$ anticommutes with $\hat{\Upsilon} = \mathrm{diag}(1, 1, 1, -1, -1, -1)$, i.e. $\hat{\Gamma}'(\boldsymbol{k})$ has chiral symmetry. This chiral symmetry can be used to make a topological characterization of $\hat{\Gamma}(\boldsymbol{k})$, since the shift proportional to $\hat{1}$ does not modify the eigenmodes.

3. Frequency dispersion and nodal line

Figure 2 shows the frequency band dispersion of the system for several values of η. Here, κ is scaled by a factor $1/\left(1 - \frac{2}{3}\eta\right)$ to remove the η dependence of the total band width. Since we have six degrees of freedom—two from the sublattices and three from the directions x, y, and z, per unit cell—we find six bands. As in the case of the single orbital tight-binding model with the diamond structure, the gap between the third and fourth bands is closed on the X–W line regardless of the value of η. (We employ the standard notation for the high symmetry points in the fcc Brillouin zone.) Around these gapless points, the gap grows linearly in the direction perpendicular to the X–W line. Actually, in the 3D Brillouin zone, the gapless points form line nodes, which are protected by the chiral symmetry. This point will be discussed in detail later. Interestingly, a new gapless point, which again forms a line node, is identified on the W–L line for $\eta < 3/4$, i.e. we can generate a line node that is absent in the single orbital tight-binding model on the diamond lattice simply by applying tension to control η.

In order to obtain a global mapping of the geometry of the line nodes in the 3D Brillouin zone, we employ the Berry phase. This is because the direct assessment of degeneracy in the eigenfrequency spectrum requires some care, and it is safer to detect a 'twist' in the eigenmodes associated with the singular degeneracy, which is captured by the Berry phase. In the numerical calculation of the Berry phase, we follow the idea in [33]. In the following, we describe the procedure to map the line nodes in order.

First, the Brillouin zone is decomposed into small cubes whose corners are specified by $\boldsymbol{k}_{\boldsymbol{l}} = (k_{l_1}, k_{l_2}, k_{l_3})$ where $\boldsymbol{l} = (l_1, l_2, l_3)$, $k_{l_\mu} = 2\pi l_\mu / N_B$, and $l_\mu = 0, \ldots, N_B - 1$. We also introduce a triplet

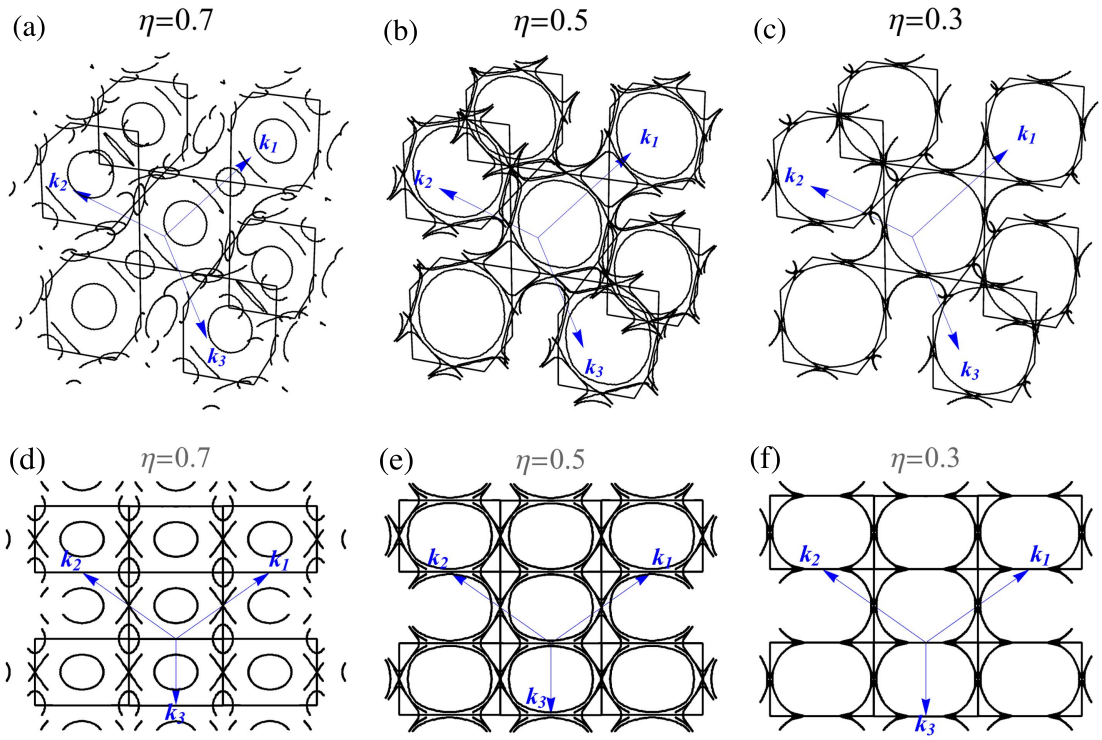

Figure 4. Line nodes for (a) $\eta = 0.7$, (b) $\eta = 0.5$ and (c) $\eta = 0.3$ viewed from a certain direction, and (d) $\eta = 0.7$, (e) $\eta = 0.5$ and (f) $\eta = 0.3$ with $\boldsymbol{k}_1$ and $\boldsymbol{k}_2$ set parallel to the paper plane.

$\psi(\boldsymbol{k}) = (|n_1(\boldsymbol{k})\rangle, |n_2(\boldsymbol{k})\rangle, |n_3(\boldsymbol{k})\rangle)$, where $|n_i(\boldsymbol{k})\rangle$ is the eigenvector of the ith band at $\boldsymbol{k}$. Here, it is a 'triplet' because we are focusing on the gap between the third and fourth bands. Then, we define a $U(1)$ link variable by

$$U_{\pm\hat{e}_\mu}(\boldsymbol{k}) \equiv \frac{1}{\mathcal{N}_{\pm\hat{e}_\mu}(\boldsymbol{k})} \det \psi^\dagger(\boldsymbol{k}) \psi\left(\boldsymbol{k} \pm \frac{\hat{e}_\mu}{N_D}\right). \tag{4}$$

Here, we have introduced a shorthand notation $\hat{e}_\mu = (2\pi/N_B)(\delta_{1\mu}, \delta_{2\mu}, \delta_{3\mu})$ and $\mathcal{N}_{\pm\hat{e}_\mu}(\boldsymbol{k}) \equiv |\det \psi^\dagger(\boldsymbol{k}) \psi\left(\boldsymbol{k} \pm \frac{\hat{e}_\mu}{N_D}\right)|$, where N_D refers to the number of discretized mesh points on each edge of each of the small cubes. Now, we can assign the Berry phase to each square surface of a small cube by taking the edge of the square as an integration path to define the Berry phase. For instance, for the square spanned by $\boldsymbol{k}_l$, $\boldsymbol{k}_l + \hat{e}_\mu$, $\boldsymbol{k}_l + \hat{e}_\nu$, and $\boldsymbol{k}_l + \hat{e}_\mu + \hat{e}_\nu$ ($\mu \neq \nu$), the assigned Berry phase is computed as

$$\begin{aligned}\tilde{\theta}_{\mu\nu}(\boldsymbol{k}_l) \equiv & \sum_{a=0}^{N_D-1} \mathrm{Arg}\, U_{\hat{e}_\mu}\left(\boldsymbol{k}_l + \frac{a}{N_D}\hat{e}_\mu\right) + \sum_{a=0}^{N_D-1} \mathrm{Arg}\, U_{\hat{e}_\nu}\left(\boldsymbol{k}_l + \hat{e}_\mu + \frac{a}{N_D}\hat{e}_\nu\right) \\ & + \sum_{a=0}^{N_D-1} \mathrm{Arg}\, U_{-\hat{e}_\mu}\left(\boldsymbol{k}_l + \hat{e}_\mu + \hat{e}_\nu - \frac{a}{N_D}\hat{e}_\mu\right) + \sum_{a=0}^{N_D-1} \mathrm{Arg}\, U_{-\hat{e}_\nu}\left(\boldsymbol{k}_l + \hat{e}_\nu - \frac{a}{N_D}\hat{e}_\nu\right).\end{aligned} \tag{5}$$

In our case, the Berry phase $\tilde{\theta}_{\mu\nu}(\boldsymbol{k}_l)$ is quantized into 0 or π (modulo 2π), owing to the chiral symmetry. Furthermore, $\tilde{\theta}_{\mu\nu}(\boldsymbol{k}_l) = \pi$ implies that there exist an odd number of Dirac points on the associated square [28, 34, 35]. From a 3D point of view, a Dirac cone on a square patch means that a line node threads through that patch. Now, if we set N_B large enough so that the possibility of multiple line nodes threading one square patch is excluded, we can follow each line node by following the Berry phase π; i.e. as far as the square patches are sufficiently small, we can draw a reasonably smooth line node by connecting the central points of the nearby patches with the Berry phase π. Note that we can always find a nearby patch with the Berry phase π when we have a certain patch with the same Berry phase, since a line node cannot be terminated abruptly.

Figure 4 illustrates the mapping of the line nodes in the 3D Brillouin zone obtained with $N_B = 151$ and $N_D = 5$. There are two classes of line nodes: the line nodes in the first class exist for any η, and their shapes are fixed and identical to those in the single orbital tight-binding model on the diamond lattice; on the other hand, the line nodes in the second class appear when η becomes smaller than a critical value $\eta_c = 3/4$. The shapes of the line nodes in the second class depend on η, and they are eventually absorbed into the line nodes in the first class at the $\eta = 0$ limit.

Before moving onto the next topic, we explain why the gapless points in our model form a line, i.e. a 1D object. Although our model is a six-band model, here we focus on a two-band effective model that is valid in the vicinity of the gap closing point. The most generic form of the effective Hamiltonian with particle-hole symmetry can be written as

$$H(\boldsymbol{k}) = \begin{pmatrix} z & x - \mathrm{i}y \\ x + \mathrm{i}y & -z \end{pmatrix} = \boldsymbol{r}(\boldsymbol{k}) \cdot \boldsymbol{\sigma}, \tag{6}$$

where $\boldsymbol{r}(\boldsymbol{k})$ is a three-dimensional vector consisting of real quantities x, y and z, and $\boldsymbol{\sigma}$ is a vector with the Pauli matrices as components. In our case, the chiral symmetry induces a constraint on $\boldsymbol{r}(\boldsymbol{k})$. For simplicity, we choose σ_3 as a chiral operator, or assume $\{H, \sigma_3\} = 0$, which restricts the Hamiltonian to the form $H(\boldsymbol{k}) = x(\boldsymbol{k})\sigma_1 + y(\boldsymbol{k})\sigma_2$. The condition of having a gap closing point is $|\boldsymbol{r}(\boldsymbol{k})| = 0$, which in fact gives two conditions, $x(\boldsymbol{k}) = 0$ and $y(\boldsymbol{k}) = 0$. That is, we have two conditions and three parameters, k_1, k_2, and k_3. Therefore, a manifold satisfying the zero gap condition has a dimension $3 - 2 = 1$, which supports the existence of the line nodes [36]. Note that the choice of σ_3 as a chiral operator does not mean loss of generality, since it is merely a matter of the basis choice.

4. Berry phase and topological edge modes

In order to relate the nontrivial topology induced by the bulk band singularity and edge modes, we calculate the Berry phase of a many-body system, whose definition is

$$\theta(k_1, k_2) = -\mathrm{i}\int_L \mathrm{Tr}\, \mathrm{d}\mathcal{A}\Big|_{k_1:\mathrm{fixed}, k_2:\mathrm{fixed}}. \tag{7}$$

Here, $\mathcal{A}$ is a non-Abelian Berry connection $\mathcal{A} = \psi^\dagger \mathrm{d}\psi$, which is a 3×3 matrix-valued one-form associated with the multiplet $\psi = (|n_1\rangle, |n_2\rangle, |n_3\rangle)$. The integration path L is taken to be a periodic path of fixed (k_1, k_2) and $0 \leqslant k_3 < 2\pi$, which is a line along the k_3-direction. Just as in the case of the previous section, the Berry phase is quantized into 0 or π due to the chiral symmetry [32]. Figures 5(a-1)–(a-5) show the Berry phase as a function of (k_1, k_2), which is obtained using the same method as in the previous section by modifying the integration path. Blue regions indicate $\theta(k_1, k_2) = 0$, while red regions indicate $\theta(k_1, k_2) = \pi$. The obtained results are consistent with the three-fold symmetry and the reflection symmetry of the diamond lattice. The lines dividing the blue and red regions are the line nodes (see figure 4) projected onto the surface under consideration, that is, the jumps in $\theta(k_1, k_2)$ are associated with the bulk singularity. The complicated structures for intermediate η can be understood by relating each of the loops on the surface to each of the line nodes in the bulk. This point will be discussed later.

If we consider a surface parallel to the plane spanned by $\boldsymbol{a}_1$ and $\boldsymbol{a}_2$, on which k_1 and k_2 are good quantum numbers, we expect at least one topologically protected edge mode for (k_1, k_2) with $\theta(k_1, k_2) = \pi$. This statement can be confirmed by investigating the edge mode explicitly. For this purpose, we consider a system which is periodic in the $\boldsymbol{a}_1$ and $\boldsymbol{a}_2$ direction, but finite in the $\boldsymbol{a}_3$ direction, so as to have the surface parallel to the $\boldsymbol{a}_1$–$\boldsymbol{a}_2$ plane, as in figure 6. Here, we apply a fixed boundary condition, where the last springs at the surface are connected to the wall. This choice of fixed boundary condition is important for maintaining 'the chiral symmetry' of the system [28]. Then, the frequency dispersion as a function of (k_1, k_2) is obtained by diagonalizing $\hat{\Gamma}_{\mathrm{edge}}(\boldsymbol{k})$, whose explicit form is

$$\hat{\Gamma}_{\mathrm{edge}}(\boldsymbol{k}) = \begin{pmatrix} \hat{\mathrm{Z}} & \hat{\Gamma}_1(\boldsymbol{k}) & & & & & & & \\ \hat{\Gamma}_1^\dagger(\boldsymbol{k}) & \hat{\mathrm{Z}} & \hat{\Gamma}_2 & & & & & & \\ & \hat{\Gamma}_2 & \hat{\mathrm{Z}} & \hat{\Gamma}_1(\boldsymbol{k}) & & & & & \\ & & \hat{\Gamma}_1^\dagger(\boldsymbol{k}) & \ddots & \ddots & & & & \\ & & & \ddots & & \ddots & & & \\ & & & & \ddots & \ddots & \hat{\Gamma}_1(\boldsymbol{k}) & & \\ & & & & & \hat{\Gamma}_1^\dagger(\boldsymbol{k}) & \hat{\mathrm{Z}} & \hat{\Gamma}_2 & \\ & & & & & & \hat{\Gamma}_2 & \hat{\mathrm{Z}} & \hat{\Gamma}_1(\boldsymbol{k}) \\ & & & & & & & \hat{\Gamma}_1^\dagger(\boldsymbol{k}) & \hat{\mathrm{Z}} \end{pmatrix}, \tag{8}$$

where $\hat{\Gamma}_1(\boldsymbol{k}) = -\kappa(\hat{\gamma}_4 + \mathrm{e}^{-\mathrm{i}\boldsymbol{k}\cdot\boldsymbol{a}_1}\hat{\gamma}_1 + \mathrm{e}^{-\mathrm{i}\boldsymbol{k}\cdot\boldsymbol{a}_2}\hat{\gamma}_2)$, $\hat{\mathrm{Z}} = \kappa(\hat{\gamma}_1 + \hat{\gamma}_2 + \hat{\gamma}_3 + \hat{\gamma}_4)$ and $\hat{\Gamma}_2 = -\kappa\hat{\gamma}_3$. Importantly, due to the fixed boundary condition, the diagonal part is uniform, which means that the eigenvectors are unaffected by the diagonal terms, and we still have a chiral symmetry in the same sense as the previous analysis.

Figures 5(b-1)–(b-5) show the frequency dispersion on a line in the surface Brillouin zone specified in figure 5(a-1), obtained using a system with 300 layers in the z-direction. We find flat in-gap modes that are

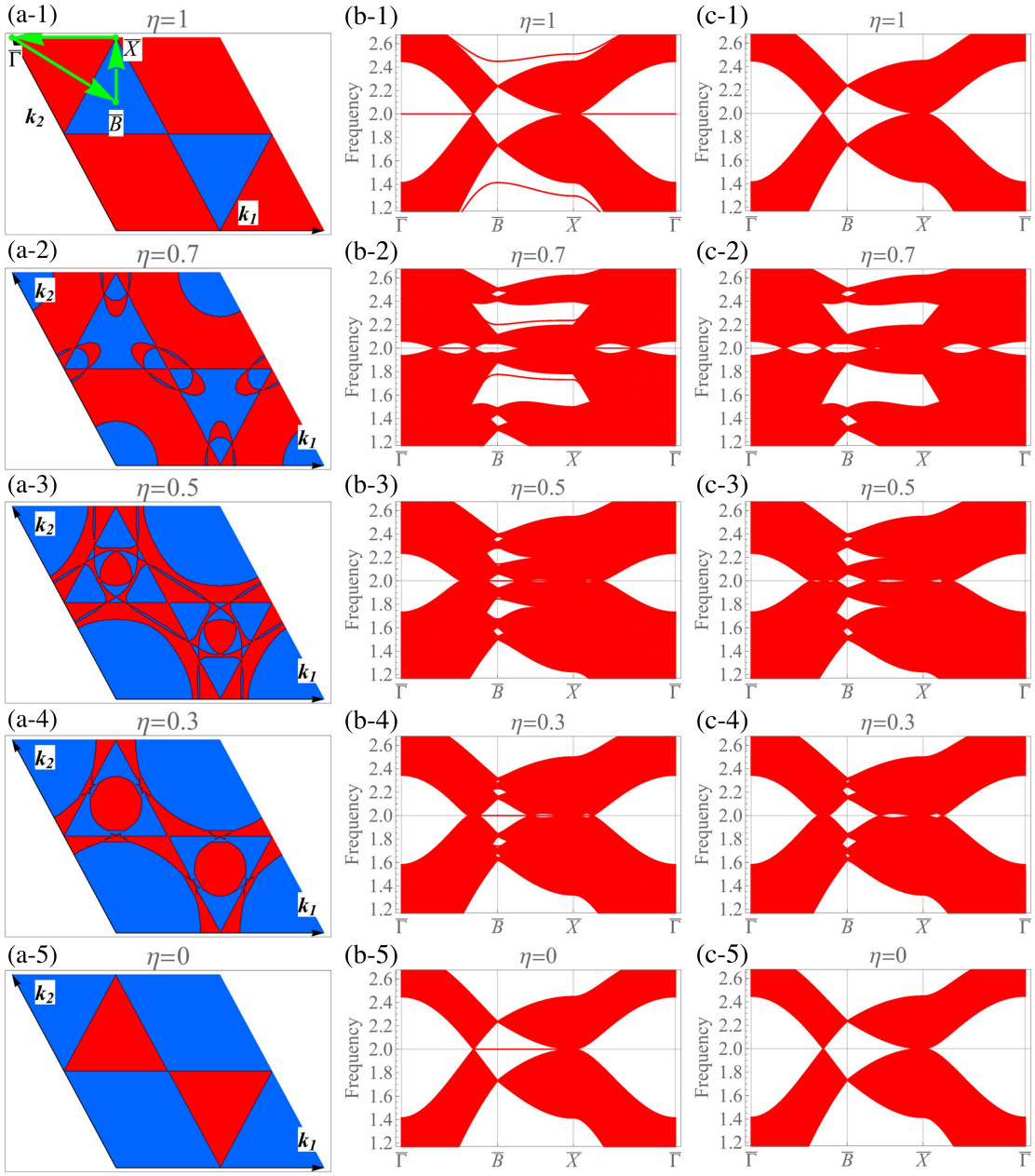

Figure 5. (a-1)–(a-5) A Berry phase diagram for (a-1) $\eta = 1$, (a-2) $\eta = 0.7$, (a-3) $\eta = 0.5$, (a-4) $\eta = 0.3$ and (a-5) $\eta = 0$. (b-1)–(b-5) The band structure with the surface for (b-1) $\eta = 1$, (b-2) $\eta = 0.7$, (b-3) $\eta = 0.5$, (b-4) $\eta = 0.3$ and (b-5) $\eta = 0$. The frequency dispersion is calculated along the lines on (a-1). (c-1)–(c-5) The band structure without a surface for (c-1) $\eta = 1$, (c-2) $\eta = 0.7$, (c-3) $\eta = 0.5$, (c-4) $\eta = 0.3$ and (c-5) $\eta = 0$.

localized at the surface in contrast with the frequency dispersion without a boundary (see figure 5(c-1)–(c-5)). As η reduces from 1 to 0, the location of the flat mode changes according to the changes in the bulk spectrum. Notably, there is only one pair of edge modes around the $\bar{\Gamma}$ point where $\theta(k_1, k_2) = \pi$ for $\eta = 1$, while there are three pairs of edge modes around the $\bar{B}$ point where $\theta(k_1, k_2) = \pi$ for $\eta = 0$. This means that if we remove the degeneracy originating in the existence of two surfaces (top and bottom), i.e. focusing on one of the surfaces, the flat edge mode for $\eta = 1$ is nondegenerate, while the one for $\eta = 0$ is three-fold degenerate.

Let us relate the edge mode and the Berry phase. Figures 7(a)–(e) show the Berry phase and the multiplicity of the pair of edge modes. As in the case of figures 5(a-1)–(a-5), the blue and red regions correspond to $\theta(k_1, k_2) = 0$ and π, respectively. From these pictures, it is found that an even number of pairs exists for the region with $\theta(k_1, k_2) = 0$, while there is an odd number of pairs for $\theta(k_1, k_2) = \pi$. It is relatively easy to understand the region with the multiplicity 0 and 1. For this region, an established argument on the relation between the Berry phase and the edge mode applies as it is. Then, the question is how to understand the region with the multiplicity 2 and 3. Intuitively, it is understood by pulling the projected loops in the 2D surface Brillouin zone back into the loops in the 3D bulk Brillouin zone. As we can see from figure 7(f), even when two

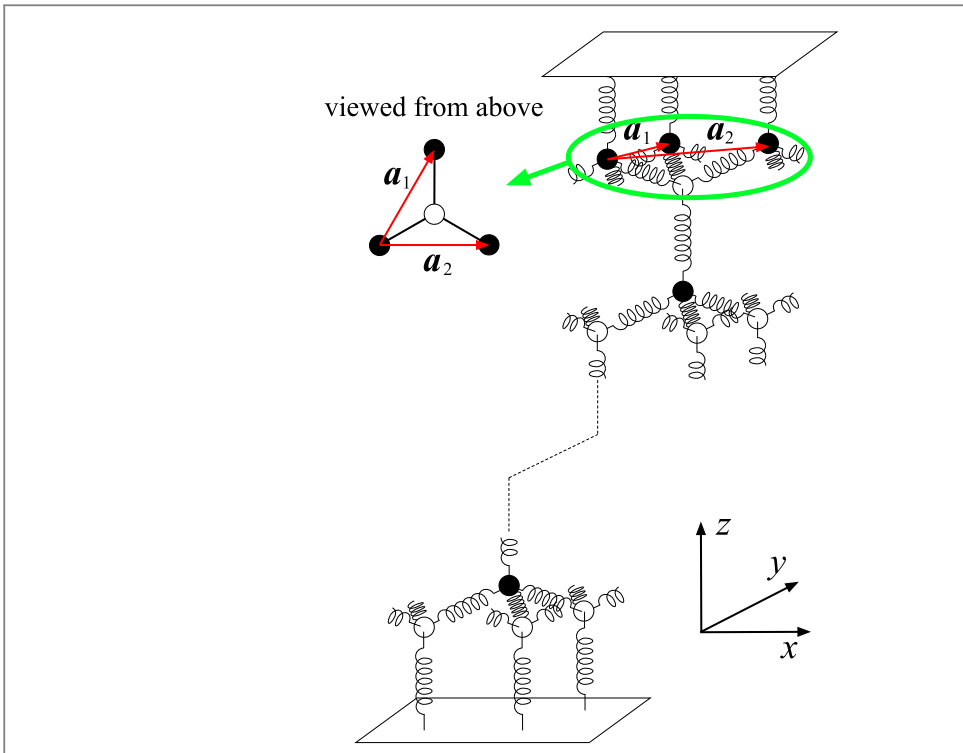

Figure 6. A schematic picture of the system with surfaces and an illustration of the fixed boundary condition.

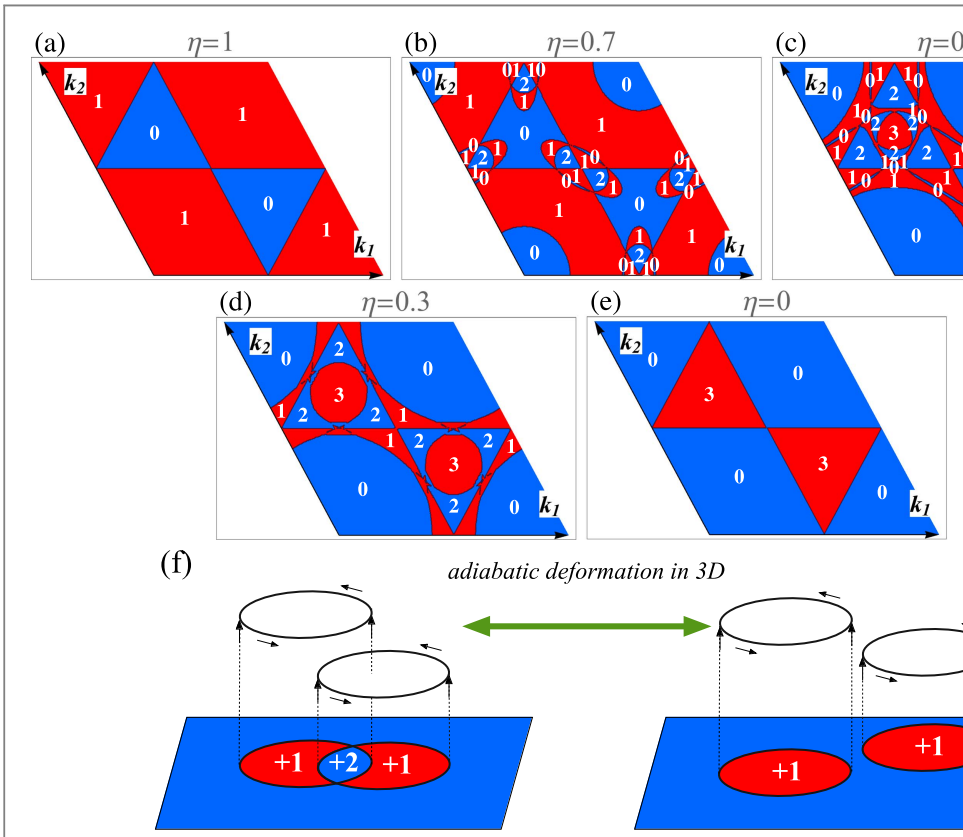

Figure 7. (a)–(e) A Berry phase diagram and the zero mode edge states for (a) $\eta = 1$, (b) $\eta = 0.7$, (c) $\eta = 0.5$, (d) $\eta = 0.3$ and (e) $\eta = 0$; the numbers denote the multiplicity of zero modes. (f) A schematic illustration of lifting 2D line node loops into the 3D Brillouin zone and deforming adiabatically; the arrows indicate the chirality of each loop, which all are the same direction.

projected loops overlap and cross each other, there is an *adiabatic* way to resolve the overlap in 3D. Assuming that each loop carries one edge mode, as in the standard argument, and any adiabatic change keeps the topological properties intact, the multiplicity larger than one can be attributed to the overlapping loops.

So far, we have been focusing on the Berry phase so as to emphasize the role of the band singularity as a source of the twist in the wave function—or eigenvector in our case. However, in order to capture the number of edge modes beyond the parity of the number of edge modes, we have to introduce the other topological invariant, which is the winding number. The definition of the winding number is made possible by the chiral symmetry. Therefore, the constant diagonal term should be subtracted before applying the following argument to our model. For a system with chiral symmetry, an appropriate choice of the basis set leads to a Hamiltonian of the form

$$H = \begin{pmatrix} 0 & \hat{\Gamma} \\ \hat{\Gamma}^{\dagger} & 0 \end{pmatrix}. \tag{9}$$

Then, the winding number is evaluated as [37]

$$N_w = -\frac{1}{2\pi}\int_L \mathrm{dArg}\,\det\hat{\Gamma}, \tag{10}$$

where the path L is taken to be the same as the path used to define the Berry phase that is $(k_1,\ k_2)$ fixed and $0 \leqslant k_3 < 2\pi$. With this choice of path, the winding number becomes a function of $(k_1,\ k_2)$. Then, it is expected that $N_w(k_1,\ k_2)$ captures the number of edge modes at $(k_1,\ k_2)$. This expectation is confirmed by our numerical calculation of N_w. Note that we have a relation $\theta = \pi N_w \ (\mathrm{mod}\ 2\pi)$, indicating that the Berry phase has an ability to capture the parity of the number of edge modes.

Generically speaking, the existence of more than one zero mode near the same boundary implies the opening of a gap (a deviation from zero energy) due to the interaction among them. However, in the present example of the nearest-neighbor spring-mass model, the edge states of each boundary have fixed chirality, χ, ($\Upsilon|\psi^{\chi}_{\mathrm{edge}}\rangle = \chi|\psi^{\chi}_{\mathrm{edge}}\rangle$, $\chi = \pm$) [38]. Then, due to the selection rule, $\langle\psi^{\pm}_{\mathrm{edge}}|(\hat{\Gamma}_{\mathrm{edge}} - \kappa\left(4 - \frac{8}{3}\eta\right)\hat{1})|\psi^{\pm}_{\mathrm{edge}}\rangle = 0$, all of the multiple zero mode edge states remain at zero energy. It justifies that the winding number itself specifies the number of edge states.

5. Summary

To summarize, we have investigated the topological properties of a mechanical diamond, which is a three-dimensional spring-mass model with a diamond structure. We have shown the interesting evolution of the gapless line nodes as a function of η, which is a parameter representing the tension of the springs in equilibrium. The structure of the line nodes in 3D is especially complicated for intermediate η. The multiplicity of the edge modes changes at the projected line nodes in the surface Brillouin zone. We have also established the bulk-edge correspondence in the mechanical diamond by relating the edge modes and two kinds of bulk topological number—the quantized Berry phase and the winding number—where the chiral symmetry plays an essential role.

Acknowledgments

This work is partly supported by Grants-in-Aid for Scientific Research, (KAKENHI), Grant numbers JP26247064, JP16K13845 from JSPS and JP25107005 from MEXT.

References

[1] Wallace P R 1947 *Phys. Rev.* **71** 622
[2] Young S M, Zaheer S, Teo J C Y, Kane C L, Mele E J and Rappe A M 2012 *Phys. Rev. Lett.* **108** 140405
[3] Wang Z, Sun Y, Chen X Q, Franchini C, Xu G, Weng H, Dai X and Fang Z 2012 *Phys. Rev.* B **85** 195320
[4] Liu Z K *et al* 2014 *Science* **343** 864
[5] Burkov A A and Balents L 2011 *Phys. Rev. Lett.* **107** 127205
[6] Wan X, Turner A M, Vishwanath A and Savrasov S Y 2011 *Phys. Rev.* B **83** 205101
[7] Burkov A A, Hook M D and Balents L 2011 *Phys. Rev.* B **84** 235126
[8] Hatsugai Y 1993 *Phys. Rev. Lett.* **71** 3697
[9] Haldane F D M and Raghu S 2008 *Phys. Rev. Lett.* **100** 013904
[10] Wang Z, Chong Y D, Joannopoulos J D and Soljačić M 2008 *Phys. Rev. Lett.* **100** 013905
[11] Prodan E and Prodan C 2009 *Phys. Rev. Lett.* **103** 248101
[12] Berg N, Joel K, Koolyk M and Prodan E 2011 *Phys. Rev.* E **83** 021913
[13] Kane C L and Lubensky T C 2014 *Nat. Phys.* **10** 39
[14] Pal R K and Ruzzene M *New J. Phys.* **19** 025001

[15] Chen B G G, Upadhyaya N and Vitelli V 2014 *Proc. Natl Acad. Sci. USA* **111** 13004
[16] Wang Y T, Luan P G and Zhang S 2015 *New J. Phys.* **17** 073031
[17] Wang P, Lu L and Bertoldi K 2015 *Phys. Rev. Lett.* **115** 104302
[18] Süsstrunk R and Huber S D 2015 *Science* **349** 47
[19] Nash L M, Kleckner D, Read A, Vitelli V, Turner A M and Irvine W T M 2015 *Proc. Natl Acad. Sci. USA* **112** 14495
[20] Paulose J, Chen B G G and Vitelli V 2015 *Nat. Phys.* **11** 153
[21] Chen B G G, Liu B, Evans A A, Paulose J, Cohen I, Vitelli V and Santangelo C D 2016 *Phys. Rev. Lett.* **116** 135501
[22] Po H C, Bahri Y and Vishwanath A 2016 *Phys. Rev.* B **93** 205158
[23] Lu L, Wang Z, Ye D, Ran L, Fu L, Joannopoulos J D and Soljačić M 2015 *Science* **349** 622
[24] Peano V, Houde M, Brendel C, Marquardt F and Clerk A A 2016 *Nat. Commun.* **7** 10779
[25] Schmidt M, Peano V and Marquardt F 2015 *New J. Phys.* **17** 023025
[26] Hafezi M and Rabl P 2012 *Opt. Express* **20** 7672
[27] Cserti J and Tichy G 2004 *Eur. J. Phys.* **25** 723
[28] Kariyado T and Hatsugai Y 2015 *Sci. Rep.* **5** 18107
[29] Socolar J E S, Lubensky T C and Kane C L *New J. Phys.* **19** 025003
[30] Wang Y T and Zhang S 2016 *New J. Phys.* **18** 113014
[31] Salerno G, Berardo A, Ozawa T, Price H M, Taxis L, Pugno N M and Carusotto I arXiv:1609.09651
[32] Ryu S and Hatsugai Y 2002 *Phys. Rev. Lett.* **89** 077002
[33] Fukui T, Hatsugai Y and Suzuki H 2005 *J. Phys. Soc. Jpn.* **74** 1674
[34] Fu L and Kane C L 2007 *Phys. Rev.* B **76** 045302
[35] Mori T 2013 *J. Phys. Soc. Jpn.* **82** 034712
[36] Blount E I 1985 *Phys. Rev.* B **32** 2935
[37] Hatsugai Y and Maruyama I 2011 *Eur. Phys. Lett.* **95** 20003
[38] Hatsugai Y, Morimoto T, Kawarabayashi T, Hamamoto Y and Aoki H 2013 *New J. Phys.* **15** 035023